Quantitative Determination of the Singlet–Triplet Energy Gap in Pseudo-Octahedral Complexes of W(IV): Measurement of the Relative π-Acidities of N-Heterocyclic Ligands

Charles E. Kriley,‡ Phillip E. Fanwick, and Ian P. Rothwell*

Contribution from the Department of Chemistry, 1393 Brown Building, Purdue University, West Lafayette, Indiana 47907-1393

Received November 1, 1993®

Abstract: The diamagnetic bis-phosphine complex $[W(OC_6H_3Ph\text{-}C_6H_4)_2(PMePh_2)_2]$ (**1**) ($OC_6H_3Ph\text{-}C_6H_4$ = cyclometallated 2,6-diphenylphenoxide) reacts rapidly in hydrocarbon solvent with nitrogen heterocyclic ligands to produce a new series of complexes $[W(OC_6H_3Ph\text{-}C_6H_4)_2(L)_2]$ (**2**: L = substituted pyridine, **3**: $(L)_2$ = substituted bipyridines; **4**: $(L)_2$ = phenanthrolines). Complexes **2**, **3**, and **4** exhibit sharp, contact-shifted ^1H NMR spectra at 25 °C, the amount of contact shifting being strongly dependent on the nature of the nitrogen donor ligand. Assignment of the signals in the ^1H NMR spectra as well as their temperature dependence indicates that a thermal equilibrium exists between a singlet ground state for the d^2-W(IV) metal center and a triplet excited state which undergoes through-bond coupling to the ligand protons. The temperature dependence of the chemical shifts of the four protons (H2, H3, H4, and H5) attached to the metalated arene rings has been used to calculate the hyperfine coupling constants and single–triplet energy gap (E) for the ligands (L) 4-*tert*-butylpyridine (E = 1138 cm^{-1}), 4-pyrrolidinopyridine (714 cm^{-1}), 4,4′-dimethyl-2,2′-bipyridine (528 cm^{-1}), and 4,4′-diphenyl-2,2′-bipyridine (362 cm^{-1}). The relative singlet–triplet energy gap for different ligands can also be estimated by measuring the amount of contact shifting of these aryl protons at 25 °C. It is found that substituents on pyridine that decrease the value of E in compounds **2** increase the value of E in complexes **3** and **4** when introduced onto the bipyridine or phenanthroline nucleus. It is argued that stronger π-acid pyridine ligands stabilize the singlet ground state by interacting with the formally d_{xy} (HOMO) orbital on the metal while stronger π-acid bipyridine and phenanthroline ligands will stabilize the d_{xz}, d_{yz} (LUMO) pair of orbitals. The fact that the *cis*-pyridine ligands in $[W(OC_6H_3Ph\text{-}C_6H_3)_2(py)_2]$ (**2a**) lie along the O–W–O (Z) axis has been confirmed by a single-crystal X-ray diffraction analysis. Crystal data at 20 °C for $WO_2N_2C_{46}H_{34}$: a = 26.299(4) Å, b = 14.802(3) Å, c = 10.1339(9) Å, β = 103.17(1)°, Z = 4 in space group $C2$.

Introduction

There has recently been considerable interest in the structure and bonding of pseudo-octahedral d^2-W(IV) complexes of the type $[W(OAr)_2Cl_2(L)_2]$ (**A**) and $[W(OR)_2Cl_2(L)_2]$ (**B**). In the case of the aryloxide complexes, both paramagnetic (OAr = 2,6-diphenylphenoxide)[1] and diamagnetic (OAr = 4-substituted phenoxides)[2] "spin isomers" have been isolated. The paramagnetic nature of the 2,6-diphenylphenoxide complex appears to be due to a sterically induced decrease in the π-donor capabilities of this ligand,[2] resulting in a smaller splitting of the three (formally t_{2g}) sets of orbitals in the pseudo-octahedral complexes. Recently Caulton et al. have structurally characterized an alkoxide analogue $[W(OCH_2CF_3)_2Cl_2(PMe_2Ph)_2]$ which is diamagnetic and which contains *trans* alkoxide ligands but mutually *cis*-phosphine and chloride groups.[3]

As an extension of our research into the organometallic chemistry of low-valent aryloxide derivatives of the early d-block metals,[4–6] we have investigated the reactivity of the diamagnetic organometallic complex $[W(OC_6H_3Ph\text{-}C_6H_4)_2(PMePh_2)_2]$ (**1**)[7] toward small molecules.[8] During this work we discovered that facile replacement of the $PMePh_2$ groups in **1** by pyridine, bipyridine, and phenanthroline ligands occurred to produce a new series of adducts that exhibit sharp, contact-shifted ^1H NMR spectra. We report here a detailed study of the structure and spectroscopic properties of this new group of compounds. This study has allowed us to accurately determine the singlet–triplet energy group in compounds of this type. Furthermore, this study not only enhances our understanding of the electronic nature of these complexes but also offers a method for determining the relative π-acceptor properties of pyridine, bipyridine, and related N-heterocyclic ligands.

Results and Discussions

Synthesis of Complexes. Previous work has shown that reduction of hydrocarbon solutions of the tungsten complex $[W(OAr)_2Cl_4]$ (OAr = 2,6-diphenylphenoxide) with sodium amalgam (4 Na per W) in the presence of $PMePh_2$ leads to the organometallic W(IV) complex $[W(OC_6H_3Ph\text{-}C_6H_4)_2(PMePh_2)_2]$ (**1**).[7] Structural studies of **1** show it to contain two cyclometallated 2,6-diphenylphenoxide ligands with mutually *trans* oxygen atoms and *cis*-$PMePh_2$ ligands. Both **1** and its PMe_2Ph derivative are diamagnetic and exhibit ^1H and ^{13}C NMR spectra which are typical for complexes containing cyclometalated 2,6-diphe-

‡ Department of Chemistry and Physics, Gyte Building, Purdue University Calumet, Hammond, IN 46323-2094.

® Abstract published in *Advance ACS Abstracts*, May 1, 1994.

(1) Kerschner, J. L.; Fanwick, P. E.; Rothwell, I. P. *Inorg. Chem.* **1989**, *28*, 780.

(2) (a) Atagi, L. M.; Mayer, J. M. *Angew. Chem., Int. Ed. Engl.* **1993**, *32*, 439. (b) Jang, S.; Atagi, L. M.; Mayer, J. M. *J. Am. Chem. Soc.* **1990**, *112*, 6413.

(3) Rothfuss, H.; Huffman, J. C.; Caulton, K. G. Submitted for publication.

(4) (a) Kerschner, J. L.; Torres, E.; Fanwick, P. E.; Rothwell, I. P.; Huffman, J. C. *Organometallics* **1989**, *8*, 1424–1430. (b) Kerschner, J. L.; Yu, J.; Fanwick, P. E.; Rothwell, I. P.; Huffman, J. C. *Organometallics* **1989**, *8*, 1414–1418. (c) Kerschner, J. L.; Fanwick, P. E.; Rothwell, I. P.; Huffman, J. C. *Inorg. Chem.* **1989**, *28*, 780–786. (d) Kerschner, J. L.; Fanwick, P. E.; Rothwell, I. P. *J. Am. Chem. Soc.* **1988**, *110*, 8235–8238.

(5) (a) Yu, J. S.; Fanwick, P. E.; Rothwell, I. P. *J. Am. Chem. Soc.* **1990**, *112*, 8171–8172. (b) Steffey, B. D.; Chamberlain, L. R.; Chesnut, R. W.; Chebi, D. E.; Fanwick, P. E.; Rothwell, I. P. *Organometallics* **1989**, *8*, 1419–1424. (c) Coffindaffer, T. W.; Steffey, B. D.; Rothwell, I. P.; Folting, K.; Huffman, J. C.; Streib, W. E. *J. Am. Chem. Soc.* **1989**, *111*, 4742–4750.

(6) (a) Durfee, L. D.; Hill, J. E.; Fanwick, P. E.; Rothwell, I. P. *Organometallics* **1990**, *9*, 75–80. (b) Durfee, L. D.; Hill, J. E.; Kerschner, J. L.; Fanwick, P. E.; Rothwell, I. P. *Inorg. Chem.* **1989**, *28*, 3095–3097.

(7) Kerschner, J. L.; Fanwick, P. E.; Rothwell, I. P. *Organometallics* **1989**, *8*, 1431–1438.

(8) Kriley, C. E.; Kerschner, J. L.; Fanwick, P. E.; Rothwell, I. P. *Organometallics* **1993**, *12*, 2051.

0002-7863/94/1516-5225$04.50/0 © 1994 American Chemical Society

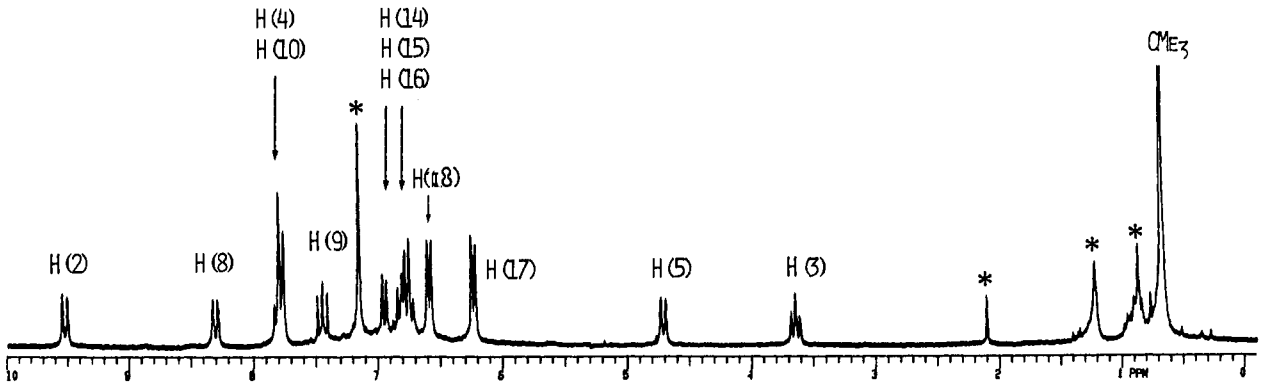

Figure 1. ^{1}H NMR spectra (C_6D_6, 30 °C) of $[W(OC_6H_3Ph\text{-}C_6H_4)_2(NC_5H_4\text{-}4Bu^t)_2]$ (**2e**). The assignment of the thirteen different proton resonances is given in the text. The solvent impurities *n*-hexane, toluene, and protio-benzene are indicated by asterisks.

Scheme 1

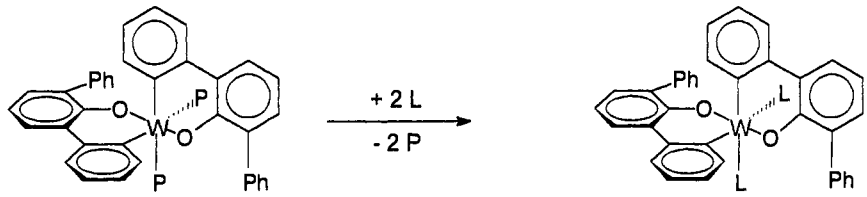

(1) P = $PMePh_2$

(2a) L = pyridine
(2b) 4-methylpyridine
(2c) 4-ethylpyridine
(2d) 4-isopropylpyridine
(2e) 4-t-butylpyridine
(2f) 3,5-dimethylpyridine
(2g) 4-phenylpyridine
(2h) 4-benzylpyridine
(2i) 3-fluoropyridine
(2j) 3-chloropyridine
(2k) 3-bromopyridine
(2l) 4-pyrollidinopyridine
(2m) 4,4'-dipyridine

(3a) 2L = 2,2'-dipyridine
(3b) 4,4'-dimethyl-2,2'-dipyridine
(3c) 4,4'-di-t-butyl-2,2'-dipyridine
(3d) 4,4'-diphenyl-2,2'-dipyridine

(4a) 2L = 1,10-phenanthroline
(4b) 3,4,7,8-tetramethyl-1,10-phen
(4c) 4,7-diphenyl-1,10-phen

nylphenoxide ligands.[7] Furthermore, these spectra are consistent with the solution structure being identical to that observed in the solid state.

The addition of a variety of pyridine, bipyridine, or phenanthroline ligands to orange benzene or toluene solutions of **1** results in the rapid formation of free $PMePh_2$ and a series of new, highly colored organometallic derivatives of W(IV) (Scheme 1). When these reactions are carried out in C_6D_6 at 25 °C and monitored by ^{1}H NMR spectroscopy, signals due to **1** decrease along with the corresponding buildup of signals due to $PMePh_2$ and the new adducts **2**, **3**, and **4**. In the case of the monodentate pyridine ligands, an intermediate complex could sometimes be observed (^{1}H NMR) in the formtion of **2** from **1**. Although not isolated and fully characterized, we believe these intermediates to be the mixed ligand complexes $[W(OC_6H_3Ph\text{-}C_6H_4)_2(PMe_2Ph)(L)]$ (L = various substituted pyridines). It was found possible to assign only some of the ^{1}H NMR resonances for these intermediates and the observed chemical shifts are consistent with the complexes being diamagnetic under ambient conditions (*vide infra*).

The signals in the ^{1}H NMR spectra of **2**, **3**, and **4** at 25 °C all appear as sharp, well-resolved resonances which are contact shifted by amounts highly dependent on the nature of the added ligand (*vide infra*, Diagram 1, Figure 1). However, addition of large excesses of ligand do not cause a change in either the width or position of these signals. Separate, well-resolved resonances for free and coordinated ligand protons are observed. Hence, exchange of free and coordinated ligands is slow on the ^{1}H NMR time scale. No reaction between 2-methylpyridine or 2,6-dimethylpyridine and **1** was observed by ^{1}H NMR, presumably due to the steric demands of these ligands. A number of the complexes **2**, **3**, and **4** were isolated from solution and purified. In the majority of cases the derivatives were generated and studied in solution by mixing **1** with the corresponding ligand.

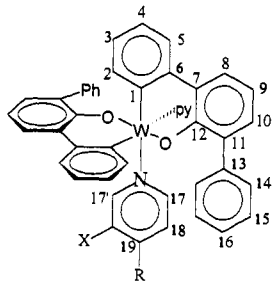

Diagram 1

Solid-State Structure of $[W(OC_6H_3Ph\text{-}C_6H_4)_2(py)_2]$ (2a). An ORTEP view of **2a** is shown in Figure 2. In Table 1 are collected selected bond distances and angles, while in Table 2 some of the structural parameters for **1**, **2a**, and other pseudo-octahedral aryloxide or alkoxide derivatives of tungsten are collected for comparison.

The coordination geometry about the W metal atom in **2a** can be seen to be very close to octahedral. The O–W–O angle of 177.1(5)° in **2a** is identical to the value of 177.0(5)° found in the corresponding $PMePh_2$ derivative **1**. The two nitrogen atoms of the pyridine ligands and two carbon atoms of the metalated

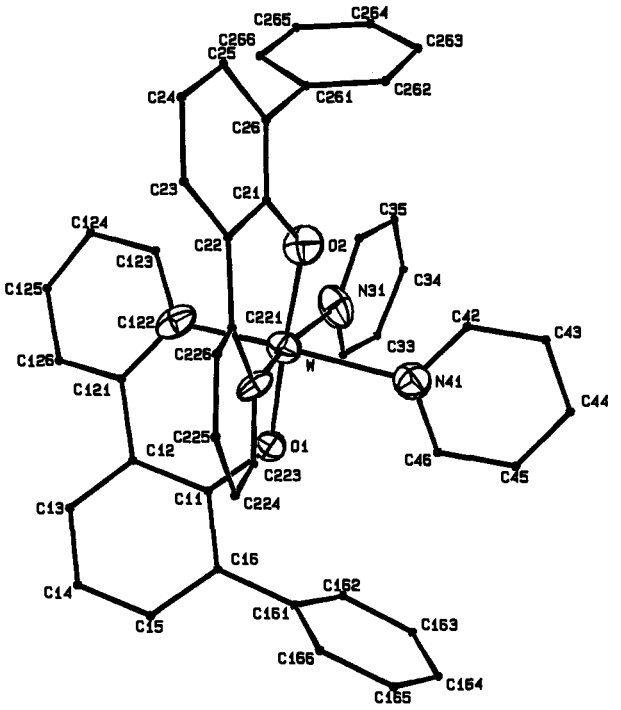

Figure 2. ORTEP view of $[W(OC_6H_3Ph\text{-}C_6H_4)_2(py)_2]$ (**2a**) emphasizing the central coordination sphere and the conformation of the pyridine ligands.

Table 1. Selected Bond Distances (Å) and Angles (deg) for $[W(OC_6H_3Ph\text{-}C_6H_4)_2(py)_2]$ (2a)

W–O(1)	1.91(1)	W–N(41)	2.29(1)
W–O(2)	1.93(1)	W–C(122)	2.09(2)
W–N(31)	2.30(1)	W–C(222)	2.14(1)
O(1)–W–O(2)	177.1(5)	O(2)–W–C(222)	87.4(5)
O(1)–W–N(31)	90.9(6)	N(31)–W–N(41)	80.9(6)
O(1)–W–N(41)	87.0(5)	N(31)–W–C(122)	88.9(6)
O(1)–W–C(122)	86.9(7)	N(31)–W–C(222)	168.8(5)
O(1)–W–C(222)	93.1(5)	N(41)–W–C(121)	168.0(5)
O(2)–W–N(31)	88.1(6)	N(41)–W–C(122)	88.9(5)
O(2)–W–N(41	90.2(6)	C(122)–W–C(222)	101.7(6)
O(2)–W–C(122)	95.8(6)		
W–O(1)–C(11)	128(1)	W–N(31)–C(32)	122(1)
W–O(2)–C(21)	132(1)	W–N(41)–C(42)	121(1)
W–N(31)–C(32)	120(1)	W–N(41)–C(46)	123(1)

Table 2. Selected Bond Distances and Angles for Pseudo-Octahedral Tungsten Complexes

	W–O, Å	W–O–C, deg	ref
cis-$[W(OC_6H_3Ph\text{-}2,6)_2Cl_4]$	1.840(3)	147.6(3)	1
	1.851(3)	144.2(3)	
trans-$[W(OC_6H_3Ph\text{-}2,6)_2Cl_3(PMe_2Ph)]$	1.877(4)		1
	1.853(4)		
$[W(OC_6H_3Ph\text{-}2,6)_2(PMe_2Ph)_2]$	1.966(4)	140.0(4)	1
$[W(OC_6H_4Me)_2Cl_2(PMePh_2)_2]$	1.848(5)	166.3(6)	2
	1.840(5)	171.7(5)	
$[W(OCH_2CF_3)_2Cl_2(PMe_2Ph)_2]$	1.844(5)	142.2(5)	3
	1.852(5)	144.8(5)	
$[W(OC_6H_3Ph\text{-}C_6H_4)_2(PMePh_2)_2]$	1.88(1)	140.7(1)	7
	1.87(1)	143.5(1)	
$[W(OC_6H_3Ph\text{-}C_6H_4)_2(py)_2]$ (**2a**)	1.91(1)	128(1)	*a*
	1.93(1)	132(1)	

[a] This work.

aryloxides make angles very close to 90° to the mutually *trans* oxygen atoms. The largest distortion from octahedral geometry involves the small N–W–N angle of 80.9(6)° and the large C–W–C angle of 101.7(6)°. This contrasts with the $PMePh_2$ derivative **1** where the P–W–P angle between two bulky phosphine ligands is opened up to 105.3(2)° and the C–W–C angle is 88.3-(7)°. The orientation of the two pyridine ligands in **2a** (Figure 2, *vide infra*) would be expected to allow easy compression of the N–W–N angle. The W–C distances of 2.09(2) and 2.14(1) Å in **2a** are similar to the values of 2.14(2) and 2.18(2) Å found in **1** while the W–N (py) distances of 2.29(1) and 2.30(1) Å are typical for pyridine ligands bound to tungsten metal centers. The W–O distances in **2a** are of most interest, especially when compared to those in the other complexes listed in Table 2. The W–O distances of 1.840(5) to 1.852(5) Å found for the aryloxide and alkoxide complexes $[W(OC_6H_4Me)_2Cl_2(PMePh_2)_2]$[2] and $[W(OCH_2CF_3)_2Cl_2(PMe_2Ph)_2)]$[3] can be taken as typical values for sterically unencumbered aryloxide or alkoxide ligands bound to W(IV) metal centers. In both of these complexes the oxygen atoms are mutually *trans*, with mutually *trans* P atoms in the aryloxide compound and mutually *cis* P atoms in the alkoxide derivative. In the case of the paramagnetic 2,6-diphenylphenoxide complex $[W(OC_6H_3Ph_2 2,6)_2Cl_2(PMe_2Ph)_2]$ the W–O distance (crystallographic inversion center) is significantly longer at 1.966-(4) Å. The W–O distances of 1.91(1) and 1.93(1) Å in **2a** are intermediate between these two distances and slightly longer than the distances of 1.87(1) and 1.88(1) Å found in the $PMePh_2$ complex **1**.

The orientation of the pyridine ligands in **2a** is of significance to the bonding discussion given below. Analysis of the torsion angles shows that the planes of both heterocyclic ligands are oriented along the O–W–O vector. The pyridine ligand bound through N(31) is essentially co-planar with the O(1)–W–O(2) axis [O(1)–W–N(31)–C(32) = –1.1°; O(1)–W–N(31)–C(36) = –179.2°; O(2)–W–N(31)–C(32) = 176.2°; O(2)–W–N(31)–C(36) = 1.8°] while the pyridine bound through N(41) is tilted only 10° from this axis [O(1)–W–N(41)–C(42) = 168.2°; O(1)–W–N(41)–C(46) = –9.1°; O(2)–W–N(41)–C(42) = –11.2°; O(2)–W–N(41)–C(46) = 171.4°].

Spectroscopic Properties. The pyridine, bipyridine, and phenanthroline derivatives **2**, **3**, and **4** display sharp, contact-shifted ^1H NMR spectra at ambient temperatures. A series of decoupling experiments allows assignment of nearly all of the resonances in the ^1H NMR spectra of these complexes (Diagram 1, Figure 1, and Table 3). The largest contact shifts are observed for the four protons attached to the metalated aryl group (Table 3). These protons alternate around the ring in being downfield H(2), H(4) or upfield H(3), H(5) shifted relative to the normal, diamagnetic aromatic region. The protons attached to the central phenoxy ring are less contact shifted, while the protons attached to the unmetalated phenyl ring are very close to the typical aromatic region of the spectrum (Table 3). The protons attached to the pyridine, bipyridine, or phenanthroline ligands also undergo contact shifting.

The magnitude of the contact shifting observed in the ambient temperature ^1H NMR spectra of **2**, **3**, and **4** is highly dependent on the nature of the nitrogen donor ligand. The most dramatically contact shifted resonances are those due to the four protons attached to the metalated aryl group. These four sets of data can be represented graphically by plotting each set of chemical shifts against each of the others. This results in the six plots shown together in Figure 3. The linearity of these plots for these four different aromatic protons implies that there is little contribution to the observed chemical shifts from dipolar (through space) interactions (*vide infra*). The alternation in direction of the contact shifts of the four protons H(2), H(3), H(4), and H(5) is consistent with the spin density from the metal being transferred through the arene ring by a hyperconjugative mechanism.[9] Further support for the lack of significant contribution to the observed contact shifts of through space, dipolar interactions comes from analysis of the chemical shifts of pyridine and 4-substituted derivatives. In unsubstituted pyridine an alteration of up-, down-, and upfield shifting of the the ortho, meta, and para protons is

(9) Delphin, W. H.; Wentworth, R. A. D. *Inorg. Chem.* **1969**, *8*, 1226.

Table 3. ^{1}H NMR Data

complexes	H2	H3	H4	H5	H8	H9	H10	H17	H18	H19	other
pyridine (**2a**)	9.84	2.56	8.17	3.67		7.53	8.10	6.13	6.34	4.69	
4-methylpyridine (**2b**)	10.19	1.48	8.54	2.76	8.04	7.63	7.99	5.84	6.25		3.24 (s, CH_3)
4-ethylpyridine (**2c**)	9.86	2.58	8.18	3.75	8.91	7.53	8.18	5.60	5.94		0.55 (t, CH_2CH_3); 3.76 (q, CH_2CH_3)
4-isopropylpyridine (**2d**)	9.65	3.30	7.94	4.40	8.26	7.50	7.82	6.11	6.45		2.65 (sept, $CHMe_2$); 0.63 (d, $CHMe_2$)
4-*tert*-butylpyridine (**2e**)	9.53	3.64	7.80	4.71	8.31	7.45	7.80	6.25	6.62		0.67 (s, CMe_3); 6.95 (H14); 6.75 (H15); 6.81 (H16)
3,5-dimethylpyridine (**2f**)	9.88	2.58	8.19	3.70	8.19	7.51	8.15	6.15		4.74	0.82 (s, CH_3)
4-phenylpyridine (**2g**)	9.48	4.04	7.78	5.09	8.36			5.75	6.12		
4-benzylpyridine (**2h**)	9.69	2.99	8.01	4.09	8.18	7.50	7.79	6.13	6.24		3.46 (s, $CH_2C_6H_5$)
3-fluoropyridine (**2i**)	9.60	3.33	7.93	4.23					4.45		
3-chloropyridine (**2j**)	9.65	3.11	8.04	4.02				6.08	5.24	6.04	
3-bromopyridine (**2k**)	9.70	2.91	8.11	3.85				6.07	5.21	6.03	
4-pyrrolidinopyridine (**2l**)	12.09	−4.39	10.62	−2.23				4.78	5.85		1.12 (m, β-CH_2); 4.04 (m, α-CH_2); 6.07 (H14); 7.49 (H15); 7.45 (H16)
4,4′-bipyridine (**2m**)	9.35	4.59	9.19	5.40				6.34	6.40		
2,2′-bipyridine (**3a**)	15.32	−14.27	14.02	−8.74							
4,4′-dimethyl-2,2′-bipyridne (**3b**)	13.56	−9.14	12.31	−4.62							1.90 (s, CH_3)
4,4′-di-*tert*-butyl-2,2′-bipyridine	18.65	−23.66	17.12	−15.79							1.45 (s, CMe_3)
4,4′-diphenyl-2,2′-bipyridine (**3d**)	17.91	−21.79	16.43	−14.39							
1,10-phenanthroline (**4a**)	14.69	−12.80	13.54	−7.71							
3,4,7,8-tetramethyl-1,10-phenanthroline	12.97	−7.62	11.83	−3.47							0.10–2.00 (s, CH_3)
4,7-diphenyl-1,10-phenanthroline	16.92	−19.18	15.69	−12.45							

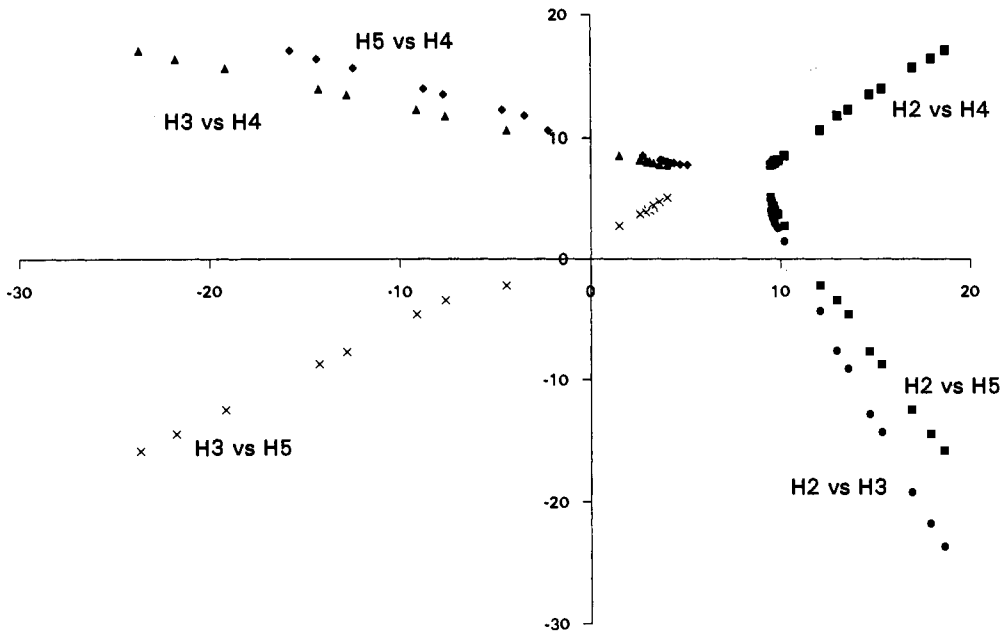

Figure 3. Plots showing the relationship between the chemical shifts (30 °C) for pairs of the aromatic protons H(2), H(3), H(4), and H(5) for all of the compounds obtained in this study (Table 4).

observed (Table 3). Replacement of the proton in the para position with a methyl group results in a downfield shift for the attached protons while the methyl protons in coordinated 4-*tert*-butylpyridine are shifted upfield. This change in the direction of contact shifts upon replacement of protons by methyl groups has been consistently used as strong evidence that through space coupling is negligible.[9]

When solutions of complexes **2**, **3**, and **4** are cooled below 30 °C there is a change in the chemical shifts of the protons toward their expected diamagnetic positions. Upon raising the temperature above 30 °C, the extent of contact shifting increases. This temperature dependence of the chemical shifts is consistent with a diamagnetic–paramagnetic thermal equilibrium for these molecules. The origin of this spin state change is clearly the d^2-tungsten metal center with a singlet ground state and triplet, thermally populated excited state.

The assessment that through-bond, contact-shift contributions dominate in these systems allows us to proceed with attempts to try and analyze the temperature dependence of the chemical shifts.[9,10] Theories for the temperature dependence of magnetic susceptibilities (Van Vleck equation) can be applied to the temperature (T) dependence of observed contact shifts. This theory predicts that the observed chemical shift (H_{obs}) should be given by the following equation

$$H_{obs} = H_{dia} - \frac{g\beta H_o A}{3kT(\gamma_H/2\pi)} \frac{(6e^{-E/kT})}{(1 + 3e^{-E/kT})} \quad (1)$$

where H_{dia} is the unperturbed, diamagnetic chemical shift, A is the hyperfine coupling constant, and E is the singlet–triplet energy gap.[11] This theoretical model has been applied not only to mononuclear systems[12] but also to dinuclear complexes involving exchange coupling between two metal centers.[13,14]

We have measured the ^{1}H NMR spectra of four compounds in toluene-d_8 solvent over a range of temperatures. The derivatives containing 4-*tert*-butylpyridine (**2e**), 4-pyrrolidinopyridine (**2l**), 4,4′-dimethyl-2,2′-bipyridine (**3b**), and 4,4′-diphenyl-2,2′-bipyridine (**3d**) were chosen for study as they exhibit different degrees

(10) Grey, E. I.; Smith, P. W. *Aust. J. Chem.* **1969**, *22*, 121.

(11) Holm, R. H.; Hawkins, C. J. In *NMR of Paramagnetic Molecules*; La Mar, G. N., Horrocks, W. D., Holm, R. H., Eds.; Academic Press: New York, 1973; Chapter 7.

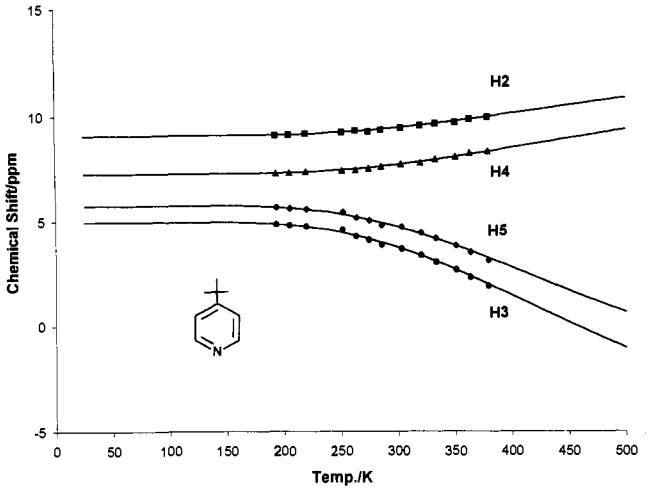

Figure 4. Plots of observed chemical shift versus temperature for the four protons H(2), H(3), H(4), and H(5) in the 4-*tert*-butylpyridine complex **2e**. The best fit curves shown correspond to eq 1 using the data in Table 5.

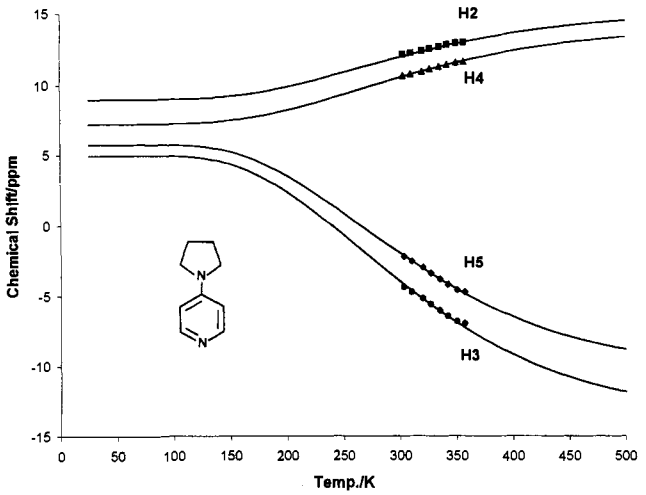

Figure 5. Plots of observed chemical shift versus temperature for the four protons H(2), H(3), H(4), and H(5) in the 4-pyrrolidinopyridine complex **2l**. The best fit curves shown correspond to eq 1 using the data in Table 5.

of contact shifting at 30 °C. For each compound the temperature dependence of the four arene protons H(2), H(3), H(4), and H(5) was fit to eq 1 by an iterative process. Although variations in A and H_{dia} for each of the four protons are to be expected, the value of the singlet–triplet energy gap (E) should be constant for this set of protons within each compound. It was found that each set of data could be reasonably fit to eq 1 and the results are shown in Figures 4–7 and Table 4. The fact that each of the four arene protons, which lie at different geometrical distances from the paramagnetic metal center, can be fit to eq 1 with a single value of E confirms that there is a negligible contribution of through-space, dipolar contact shifts.[13]

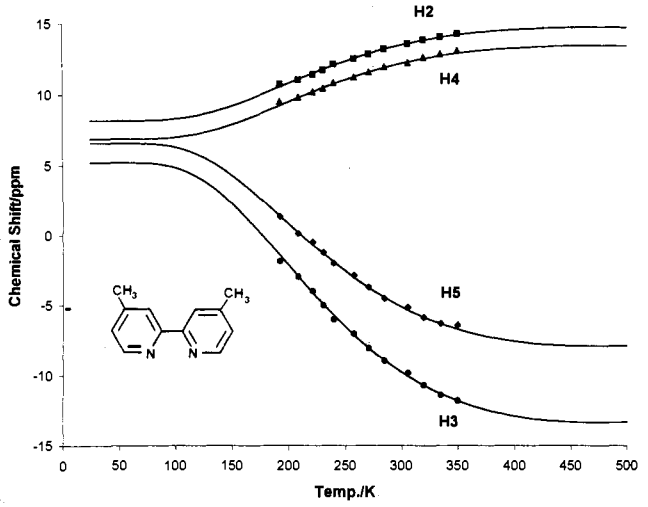

Figure 6. Plots of observed chemical shift versus temeprature for the four protons H(2), H(3), H(4), and H(5) in the 4,4′-dimethylbipyridine complex **3b**. The best fit curves shown correspond to eq 1 using the data in Table 5.

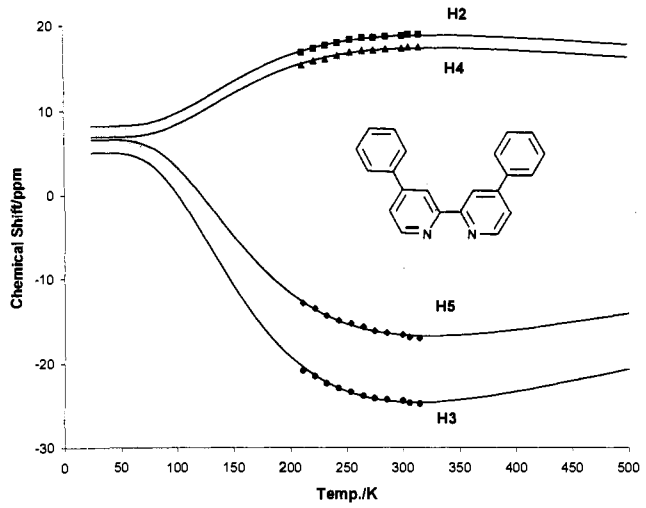

Figure 7. Plots of observed chemical shift versus temperature for the four protons H(2), H(3), H(4), and H(5) in the 4,4′-diphenylbipyridine complex **3d**. The best fit curves shown correspond to eq 1 using the data in Table 5.

The values of the hyperfine coupling constants (A) and the diamagnetic chemical shift (H_{dia}) do not vary significantly for each of the four individual arene protons as one changes the donor ligand. This is to be expected if there is no dramatic change in the bonding of the cyclometalated 2,6-diphenylphenoxide ligand for the four complexes used in this study. Furthermore, the linearity of the plots shown in Figure 3 is to be expected if the compounds obey eq 1 and the hyperfine coupling constants for each of the individual protons do not vary significantly from compound to compound. The slope of the lines in Figure 3 would hence approximate to the ratio of hyperfine coupling constants, A(H2)/A(H3) etc. The gradients obtained from Figure 3 agree reasonably well with the values of A (Table 4) obtained from the temperature dependence of the ^{1}H NMR spectra.

Given the similarity in the values of the hyperfine coupling constants (A) found for proton H2 in Table 4, it is possible to use eq 1 to graphically show how the chemical shift of H2 at 25 °C will vary as the singlet–triplet energy gap (E) changes. This behavior is shown in Figures 8 and 9. From these plots it is possible to estimate the values of E for all of the complexes obtained

(12) (a) Bleany, B.; Bowers, K. D. *Proc. R. Soc. London* **1952**, *A214*, 451. (b) Shaw, B. D.; Moss, J. R. *J. Chem. Soc. A* **1970**, 595. (c) Butcher, A. V.; Chatt, J.; Leigh, G. J.; Richards, P. L. *J. Chem. Soc., Dalton Trans.* **1972**, 1064. (d) Randall, E. W.; Shaw, P. *Mol. Phys.* **1965**, *10*, 41. (e) Chatt, J.; Leigh, G. J.; Mingos, D. M. P.; Randall, E. W.; Shaw, D. *Chem. Commun.* **1968**, 419.

(13) (a) Coffindaffer, T. W.; Niccolai, G. P.; Powell, D.; Rothwell, I. P.; Huffman, J. C. *J. Am. Chem. Soc.* **1985**, *107*, 3572. (b) Hodgson, D. J. *Prog. Inorg. Chem.* **1975**, *19*, 173. (c) Hatfield, W. E.; MacDougal, J. J.; Shepherd, R. E. *Inorg. Chem.* **1981**, *20*, 4216. (d) Boyd, P. D. W.; Smith, T. D. *Inorg. Chem.* **1971**, *10*, 2041. (e) Earnshaw, A.; Lewis, J. *J. Chem. Soc.* **1961**, 396. (f) Hopkins, M. D.; Zieflow, T. C.; Miskowski, V. M.; Gray, H. B. *J. Am. Chem. Soc.* **1985**, *107*, 510.

(14) (a) Cotton, F. A.; Eglin, J. L.; Hong, B.; James, C. A. *J. Am. Chem. soc.* **1992**, *114*, 4915. (b) Cotton, F. A.; Chen, H.; Daniels, L. M.; Feng, X. *J. Am. Chem. Soc.* **1992**, *114*, 8980.

Table 4. Values of Single–Triplet Energy Gap (E), Hyperfine Coupling Constant (A), and Diamagnetic Chemical Shift (H_{dia}) for the Protons H2, H3, H4, and H5 Obtained from the Curves Fit in Figures 4–7

		E/cm-1		H(2)	H(3)	H(4)	H(5)
(2e)	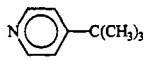	1138	A/MHz	-0.408	1.41	-0.49	1.20
			Hdia/ppm	9.09	4.95	7.26	5.75
(2l)	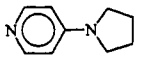	714	A/MHz	-0.463	1.44	-0.515	1.25
			Hdia/ppm	9.09	4.95	7.26	5.75
(3b)	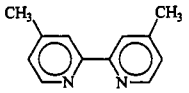	528	A/MHz	-0.39	1.11	-0.39	0.87
			Hdia/ppm	8.2	5.2	6.9	6.6
(3d)	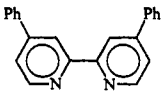	358	A/MHz	-0.433	1.17	-0.425	0.96
			Hdia/ppm	8.2	5.0	6.9	6.6

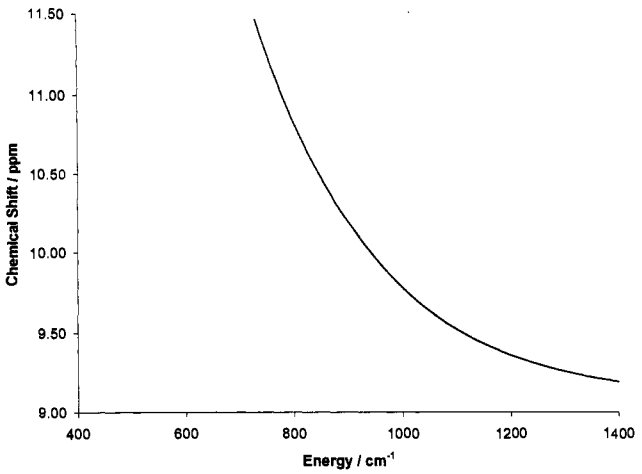

Figure 8. Plot of chemical shift of proton H(2) versus the single–triplet energy gap (E) according to eq 1 using A = –0.408 MHz and $H(2)_{dia}$ = 9.09 ppm.

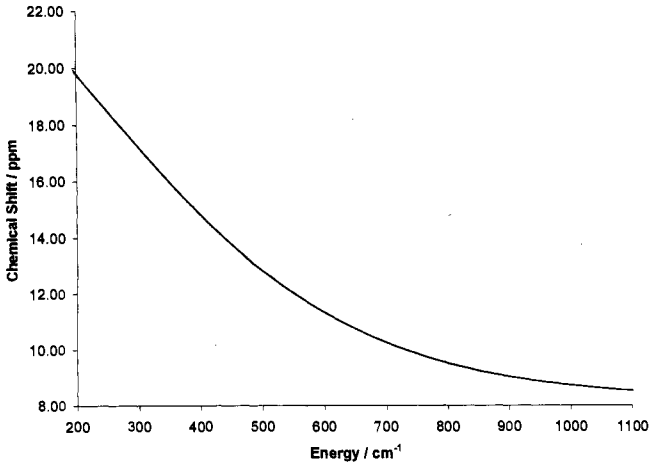

Figure 9. Plot of chemical shift of proton H(2) versus the singlet–triplet energy gap (E) according to eq 1 using A = –0.39 MHz and $H(2)_{dia}$ = 8.2 ppm.

in this study by simply using the chemical shift of H2 measured at 30 °C (Table 3). The values of E (cm^{-1}) estimated in this fashion are collected in Table 5. It can be seen (Tables 4 and 5) that the magnitude of the singlet–triplet energy gap is strongly dependent on the nature of the donor ligand, and this is discussed in detail below.

Table 5. Values of the Singlet–Triplet Energy Gap (E) Estimated by Using Eq 1 and the Curves in Figures 8 and 9[a]

		E/cm-1			E/cm-1
(2m)	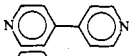	1205	(4p)	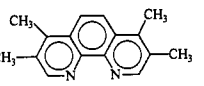	553
(2g)	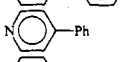	1120			
(2e)	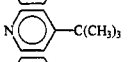	1098 (1138)	(3b)	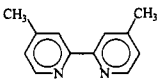	523(528)
(2i)	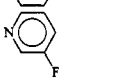	1064			
(2d)	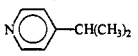	1043	(4a)	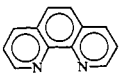	473
(2j)	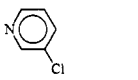	1043	(3a)	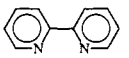	447
(2h)	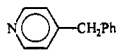	1030			
(2k)	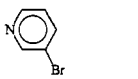	1028	(4c)	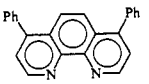	387
(2a)		981			
(2c)	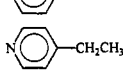	976	(3d)	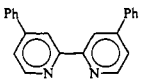	354(358)
(2f)	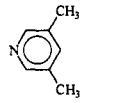	971			
(2b)	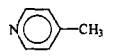	899	(3c)	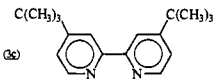	329
(2l)	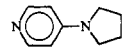	676(714)			

[a] The values in parentheses are the values obtained in Table 4 by curve fitting to the temperature-dependent ^{1}H NMR spectra.

Theoretical Discussion. The analysis of the electronic structure of these pseudo-octahedral complexes initially focuses on the three, nondegenerate set of orbitals that would be the purely metal based t_{2g} set for an octahedral complex with no π-bonding. The splitting of these three orbitals in complexes of the type **2**, **3**, and

4 will be as shown (Diagram 2) with the *z*-axis lying along the

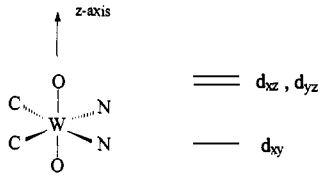

Diagram 2

O–W–O vector. The orbitals designated d_{xz} and d_{yz} will be raised in energy above the d_{xy} orbital due to π-donation from the oxygen atoms of the cyclometalated aryloxide ligands. A similar situation is to be expected for complexes of the type $[W(OAr)_2Cl_2(L)_2]$, and the observation of high- and low-spin isomers has been attributed to the degree of π-donation of the aryloxide ligand.[2] The contact-shifted ^{1}H NMR spectra observed for complexes **2**, **3**, and **4** as well as their temperature dependence can, therefore, be ascribed to a thermal equilibrium between the diamagnetic singlet ground state (both electrons in the formally d_{xy} orbital) and the paramagnetic triplet excited state with one of the electrons promoted to either the d_{xz} or d_{yz} orbital.

The results obtained in Table 4 show that the singlet–triplet gap in these complexes is highly sensitive to the nature of the pyridine, bipyridine, or phenanthroline ligand that is coordinated. This effect can be ascribed to the varying π-acceptor properties of these ligands. In the case of the monodentate pyridine ligands, the solid-state structure of **2a** shows the two pyridine rings to be oriented along the O–W–O (*z*) axis (Figure 2). This orientation is of the correct symmetry to allow back-bonding from the d_{xy} orbital on tungsten into the π^*-orbital of the pyridine ligands. The effect of this π-bonding will be to lower the level of the d_{xy} orbital, thus stabilizing the singlet ground state. This bonding picture predicts that the largest singlet–triplet energy gap, and hence the smallest amount of contact shifting, will occur for the strongest π-acceptor pyridine ligands. It can be seen, Tables 3 and 5, that this is the case. The smallest amount of contact shifting at 30 °C is found for the ligands 4-phenylpyridine and 4,4′-dipyridyl. The presence of the aromatic group in the 4-position is expected to stabilize the π^*-orbital of the nitrogen heterocycle. Previous work by our group has shown that in the complex $[Ti(OAr)_2(py\text{-}4Ph)_3]$ the solid-state structure clearly shows one of the 4-phenylpyridine ligands to have undergone significant π-back-bonding with the family d^2-Ti(II) metal center.[15] The largest contact shifts at 30 °C observed for a pyridine complex are obtained with the ligand 4-pyrrolidinopyridine. The π-donating 4-pyrrolidino substituted will be expected to decrease the π-acidity of the pyridine nucleus. The singlet–triplet energy gap was calculated for this complex to be 714 cm^{-1}, much less than the value of 1,138 cm^{-1} measured for the 4-*tert*-butylpyridine complex (Table 4).

The bipyridine and phenanthroline complexes **3** and **4**[16] exhibit larger amounts of contact shifting at 30 °C (Table 3). The physical structure of these bidentate ligands dictates that their arene rings will be perpendicular to the O–W–O vector, i.e. rotated 90° from that found for the bis(pyridine) series. Overlap between the π^*-orbital of the heterocyclic ring and the d_{xz}, d_{yz} orbitals on the metal can now take place. Hence, it is expected that as a series, bipyridine and phenanthroline ligands will cause a smaller singlet–triplet energy gap than for pyridine ligands. Furthermore, substituents which increase the π-acceptor properties of the bipyridine or phenanthroline nucleus will decrease the singlet–triplet energy gap. This is exactly the reverse of the situation predicted for simple pyridine ligands. It can be seen (Table 5) that the energy gap is 528 cm^{-1} in the 4,4-dimethyl-2,2′-bipyridine complex and drops to 362 cm^{-1} for the 4,4′-diphenyl derivative. It is also clear (Table 3) that substituents on pyridine which lead to smaller amounts of contact shifting cause the opposite effect when attached to the bipyridine or phenanthroline nucleus.

Within the pyridine series, Table 5, the introduction of a halogen into the metaposition causes an increase in the singlet–triplet energy gap consistent with a more π-basic pyridine nucleus. The trend observed for simple alkyl-substituted pyridines is not so readily rationalized, however. Introduction of a single methyl group in the para position leads to a smaller singlet–triplet energy gap of 899 cm^{-1} for **2b** compared to 981 cm^{-1} for **2a**, consistent with the electron-releasing methyl group slightly decreasing the π-acidity of the pyridine nucleus. The successive introduction of β-methyl groups within the 4-alkyl substituent, however, leads to a decrease in π-acidity as judged by the estimated energy gap: cf. 899 cm^{-1} for 4-CH_3, 976 cm^{-1} for 4-CH_2CH_3, 1043 cm^{-1} for 4-$CH(CH_3)_2$, and 1098 cm^{-1} (1138 cm^{-1}) for 4-$C(CH_3)_3$. An identical trend is observed for alkyl-substituted bipyridine ligands where 4,4′-dimethylbipyridine is a weaker π-acid than bipyridine when judged by the larger singlet–triplet energy gap whereas the 4,4′-di-*tert*-butylbipyridine ligand causes the smallest energy gap, implying a better π-accepting ligand. This difficulty in correlating the chemical shifts of complexes containing alkyl-substituted ligands highlights the fact that although π-bonding considerations may be dominant, there are other effects (in particular σ-bonding) that will influence the values of the singlet–triplet energy gap.

We have attempted to determine the magnetic susceptibilities of these complexes in solution using the Evan's method. However, the solubility of the complexes in benzene and toluene is too low for reliable values to be obtained. As an example, the room temperature magnetic moment of the pyridine complex **2a** was determined to be 1.5(5) μ_B in benzene solution using the Evan's method. This value is close to that predicted by the Van Vleck

Table 6. Crystal Data and Data Collection Parameters

formula	$WO_2N_2C_{46}H_{34}$
formula wt	830.65
space group	C2 (No. 5)
a, Å	26.299(4)
b, Å	14.802(3)
c, Å	10.1339(9)
β, deg	103.17(1)
V, Å^3	3841(2)
Z	4
d_{calc}, g cm^{-3}	1.436
cryst dimens, mm	0.39 × 0.28 × 0.04
temp, deg C	20.
radiation (wavelength)	Mo Kα (0.71073 Å)
monochromator	graphite
linear abs coeff, cm^{-1}	31.08
absorption corr applied	empirical[a]
transmission factors: min, max	0.74, 1.00
diffractometer	Enraf-Nonius CAD4
scan method	ω–2θ
h, *k*, *l* limits	0 to 28; 0 to 15; –10 to 10
2θ range, deg	4.00–45.00
scan width, deg	0.53 + 0.35 tan (θ)
take-off angle, deg	2.95
programs used	Enraf-Nonius MolEN
F_{000}	1656.0
p-factor used in weighting	0.040
data collected	2631
unique data	2631
data with $I > 3.0\sigma(I)$	2191
no. of variables	399
largest shift/esd in final cycle	0.05
R	0.033
R_w	0.044
goodness of fit	1.189

[a] Walker, N.; Stuart, D. *Acta Crystallogr., Sect. A* **1983**, *A39*, 158.

(15) Durfee, L. D.; Hill, J. E.; Kerschner, J. L.; Fanwick, P. E.; Rothwell, I. P. *Inorg. Chem.* **1989**, *28*, 3095.

(16) for a discussion of the ability of bipyridine ligands to π-accept from "$M(OR)_2$" centers see: (a) Chisholm, M. H.; Kober, E. M.; Ironmonger, D. J.; Thornton, P. *Polyhedron* **1985**, *4*, 1869. (b) Chisholm, M. H.; Huffman, J. C.; Rothwell, I. P.; Bradley, P. G.; Kress, N.; Woodruff, W. H. *J. Am. Chem. Soc.* **1981**, *103*, 4945 and references therein.

equation with a singlet–triplet energy gap equal to that estimated for **2a**. The solubility of **2a** in benzene is high enough for well-resolved ^{1}H NMR spectra to be obtained but a saturated solution of **2a** only results in a separation of a few hertz between solvent benzene and a reference sample. Hence, there is a very large error in the values of the magnetic moment obtained in this fashion.

Experimental Section

All operations were carried out under a dry nitrogen atmosphere or in vacuo either in a Vacuum Atmosphere Dri-Lab or by standard Schlenk Techniques. Hydrocarbon solvents were dried by distillation from sodium benzophenone. The compound $[W(OC_6H_3Ph\text{-}C_6H_4)_2(PMePh_2)_2]$ was obtained by previously reported procedures.[7] Routine ^{1}H NMR and variable-temperature ^{1}H NMR spectra were recorded on Gemini 200 and Varian 200 XL spectrometers and are referenced to Me_4Si by using the protio impurities of commercial benzene-d_6 or toluene-d_8 as internal standards. The synthetic procedures used to obtain the pyridine, bipyridine, and phenanthroline adducts are similar. A representative outline is given below.

Preparation of $[W(OC_6H_3Ph\text{-}C_6H_4)_2(C_5H_5N)_2]$ (2a). To 50 mL of a benzene solution of $[W(OC_6H_3Ph\text{-}C_6H_4)_2(PMePh_2)_2]$ (1.00 g, 0.93 mmol) was added C_5H_5N (0.16 g, 2.03 mmol). An immediate color change of orange to purple was observed upon the addition of pyridine. The solution was left to stir overnight under a nitrogen atmosphere. Removal of solvent under vacuum yielded the crude product as a purple solid. Small crysals of $[W(OC_6H_3Ph\text{-}C_6H_4)_2(C_5H_5N)_2]$ were isolated from a concentrated 1:1 benzene/hexane mixture.

An identical procedure was used to obtain **2b**, **2c**, **2e**, **2l**, **3a**, and **4a**. All of the other complexes were generated in solution by mixing $[W(OC_6H_3Ph\text{-}C_6H_4)_2(PMePh_2)_2]$ (**1**) with the corresponding ligand in C_6D_6 or $C_6D_5CD_3$ solvent and analyzed by ^{1}H NMR.

Crystal Structure of $[W(OC_6H_3Ph\text{-}C_6H_4)_2(py)_2]$ (2a). Crystal data and data collection parameters are collected in Table 6. Further details of the crystal structure determination are contained in the supplementary material.

Acknowledgment. We thank the National Science Foundation (Grant CHE-9321906) for financial support of this research and Professor D. R. McMillin and the referees of this paper for extremely helpful suggestions.

Supplementary Material Available: Description of experimental procedures and tables of bond distances and angles and fractional coordinates for **2a** (25 pages); listing of observed and calculated structure factors (10 pages). This material is contained in many libraries on microfiche, immediately follows this article in the microfilm version of the journal, and can be ordered from the ACS; see any current masthead page for ordering information.